Hybridization and electron-phonon coupling in ferroelectric $BaTiO_3$ probed by resonant inelastic x-ray scattering

S. Fatale,[1] S. Moser,[2] J. Miyawaki,[3,4] Y. Harada,[3,4] and M. Grioni[1]

[1]*Institute of Physics (IPHYS), École Polytechnique Fédérale de Lausanne (EPFL), CH-1015 Lausanne, Switzerland*

[2]*Advanced Light Source (ALS), Berkeley, California 94720, USA*

[3]*Institute for Solid State Physics (ISSP), University of Tokyo, Kashiwanoha, Kashiwa, Chiba 277-8526, Japan*

[4]*Synchrotron Radiation Research Organization, University of Tokyo, Sayo-cho, Sayo, Hyogo 679-5198, Japan*

(Received 14 September 2016; revised manuscript received 19 October 2016; published 16 November 2016)

We investigated the ferroelectric perovskite material $BaTiO_3$ by resonant inelastic x-ray scattering (RIXS) at the Ti L_3 edge. We observe with decreasing temperature a transfer of spectral weight from the elastic to the charge-transfer spectral features, indicative of increasing Ti $3d$-O $2p$ hybridization. When the incident photon energy selects transitions to the Ti $3d$ e_g manifold, the quasielastic RIXS response exhibits a tail indicative of phonon excitations. A fit of the spectral line shape by a theoretical model allows us to estimate the electron-phonon coupling strength $M \sim 0.25$ eV, which places $BaTiO_3$ in the intermediate coupling regime.

DOI: 10.1103/PhysRevB.94.195131

I. INTRODUCTION

$BaTiO_3$ is a much studied ferroelectric perovskite, of special interest for its high paraelectric to ferroelectric transition temperature $T_C \sim 390$ K and for many practical applications [1]. It has a high-temperature cubic structure, which successively becomes tetragonal at T_C, then orthorhombic at 280 K, and finally rhombohedral below 190 K. Although $BaTiO_3$ is often referred to as a paradigmatic ferroelectric, the nature of the paraelectric to ferroelectric transition is not of the usual displacive type, where the distortion—and the associated macroscopic electric polarization—grows from zero below T_C. Already in the paraelectric phase x-ray diffraction shows diffuse lines, indicative of one-dimensional correlations along the ⟨100⟩ directions, condensing into Bragg peaks only at low temperature [2]. Local structural and electronic probes such as extended x-ray absorption fine structure (EXAFS) and x-ray absorption spectroscopy (XAS) [3,4] suggest that the TiO_6 octahedra—the basic building blocks of this material—locally exhibit a rhombohedral distortion at all temperatures. The presence of a distortion is consistent with the observation of Raman modes forbidden in cubic symmetry [5]. Accurate neutron measurements of the ionic pair distribution function [6] indeed support an alternative order-disorder model for the transition originally proposed by Comès [2]. In this scenario, the Ti ions are always displaced along one of the equivalent ⟨111⟩ directions towards the faces of the octahedra. At high temperature the distortions and the associated electric dipoles are randomly oriented, and the macroscopic polarization is zero. Nevertheless, the projections of the local distortions along the ⟨100⟩ Ti-O-Ti directions exhibit a strong correlation [2]. With decreasing temperature, transverse coherence is first achieved at T_C for one component, and then for the remaining two components in the orthorhombic and finally in the rhombohedral phase [6].

Ferroelectricity is typically observed in oxides containing transition metal (TM) ions with a d^0 configuration. On general grounds, the driving force for the distortion is the energy gained when the increased TM-O hybridization lowers the occupied—mostly O-derived—bonding states, while the mostly TM-derived unoccupied antibonding states are raised at no energy cost [7]. This is supported quantitatively for $BaTiO_3$ by first-principles band structure calculations for the undistorted and distorted structures [8,9]. Experimentally, XAS measurements at the Ti L-edge [10] and Ti K-edge [11] probe the Ti $3d$-O $2p$ hybridization, but, owing to the large core-hole potential in the final state, atomiclike multiplet effects and changes in the electronic wave functions, strongly influence the results. The former can be effectively described in model calculations; the latter are more difficult to determine quantitatively. Hybridization effects on the band structure can in principle be investigated by angle-resolved photoemission (ARPES), which, however, suffers from a large surface sensitivity and from charging effects in insulating materials.

Resonant inelastic x-ray scattering (RIXS) is immune to these difficulties [12]. As a photon-in–photon-out spectroscopy it is a bulk-sensitive probe of the electronic structure of metals and insulators. It shares the site and chemical sensitivity of XAS, but the core hole, which is present in the RIXS intermediate state—the final state of XAS—is absent in the RIXS final state, and therefore does not affect the relevant valence band excitations. RIXS is a powerful probe of the electronic structure of solids and of collective magnetic excitations, namely in cuprate materials [13]. RIXS can also access vibrational excitations in molecules [14] and solids [15], and the strength of the electron-phonon (e-ph) coupling can be extracted from an analysis of the spectral line shape [16,17]. Recently, hard x-ray RIXS measurements have been performed on $BaTiO_3$ and the results confirm the partial delocalization of the Ti $3d$ states [18]. In this paper, we exploit RIXS at the Ti L_3 ($2p_{3/2} \rightarrow 3d$) edge to probe the electronic states of $BaTiO_3$. We monitor the temperature evolution of a prominent spectral feature associated with charge-transfer excitations across the fundamental energy gap. We find that the Ti-O hybridization steadily increases from high to low temperature, with no apparent discontinuity at T_C. Moreover, from a line-shape analysis of the quasielastic response with recent theory based on the Fröhlich Hamiltonian, we find evidence of an intermediate coupling to a 65 meV TO phonon mode.

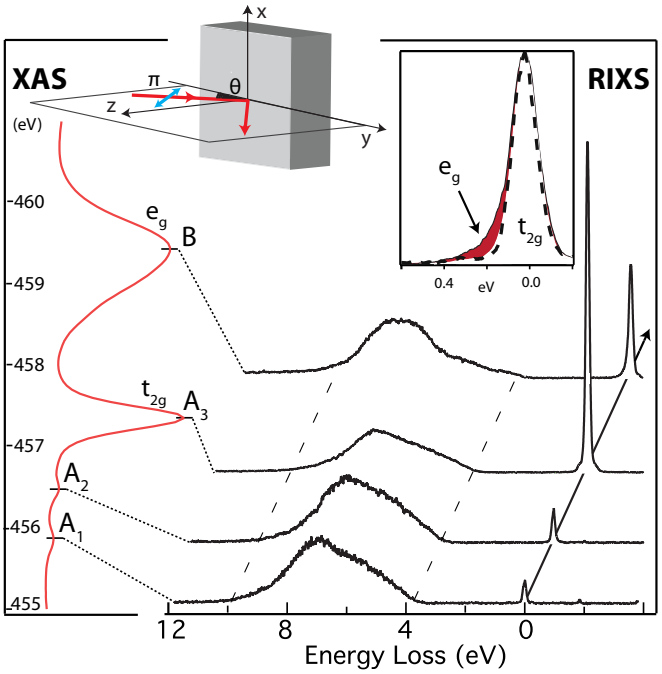

FIG. 1. (Left) Ti L_3 XAS spectrum of $BaTiO_3$. (Right) RIXS data measured at selected incident photon energies. The inset shows a comparison of the quasielastic response measured in correspondence of the A_3 (t_{2g}) and B (e_g) features of the XAS spectrum. The dashed black line is the elastic peak measured on a reference Cu sample.

II. EXPERIMENTAL

We performed Ti L_3 edge ($2p_{3/2} \rightarrow 3d$) RIXS measurements at the HORNET end station at beam line BL07LSU of SPring-8 [19]. The $BaTiO_3$ single crystal was purchased from Crystal GmbH and oriented with the normal to the polished (001) surface within the horizontal scattering plane, as sketched in the inset of Fig. 1. We used π-polarized light with an incidence angle $\theta = 55^\circ$ and a fixed scattering angle of 90°, corresponding to a transferred wave vector $q = 0.33$ Å^{-1} at 10° from the (001) ferroelectric axis. The energy resolution, determined from the width of the elastic peak measured on polycrystalline copper, was $\Delta E = 135$ meV. XAS data were collected in the total fluorescence yield mode.

III. RESULTS AND DISCUSSION

Figure 1 presents the Ti L_3 XAS of $BaTiO_3$ (left) and an overview of the RIXS data (right). The XAS line shape is typical for a Ti^{4+} (d^0) ion in an octahedral environment [20]. It represents transitions from the $3d^0$ ground state to $\underline{c}3d^1$ final states, where $\underline{c}$ stands for a $2p_{3/2}$ core hole. It exhibits two weak preedge features (A_1, A_2) and two prominent features A_3 (457.5 eV) and B (459.5 eV), which correspond to transitions to t_{2g} and, respectively, e_g crystal field states. Peak A_3 is sharp, owing to a strong excitonic character. Peak B is broader, reflecting the larger bandwidth of the e_g states and a weaker interaction with the core hole [17,21].

The XAS final states correspond to the intermediate states of the RIXS process. RIXS spectra measured in correspondence of the A_1, A_2, A_3, and B XAS features are shown as a function of the energy loss $E = (h\nu_{in} - h\nu_{out})$, the difference between the energies of the incident and scattered photons. The peak at $E = 0$ represents the quasielastic response, containing the elastic peak, for which the final state coincides with the initial state, and unresolved phononic energy losses, to be discussed later. The broad feature between 4 eV and 10 eV represents charge-transfer (CT) excitations, where an electron is excited across the fundamental energy gap from the full oxygen-derived valence band to the empty Ti-derived conduction band. The clean gap between the elastic peak and the CT feature reflects the absence of dd excitations, consistent with the formal d^0 configuration of the Ti ion. This observation confirms that the density of Ti^{3+} impurities, which are associated with O vacancies, is extremely small in our sample.

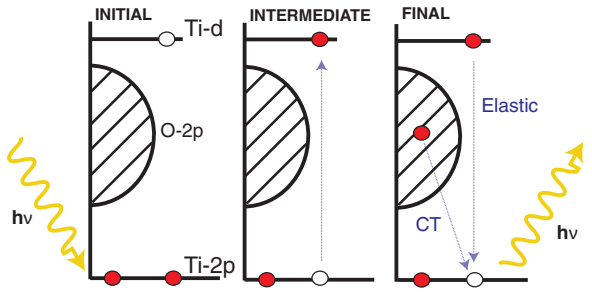

FIG. 2. Schematic representation of the RIXS process occurring in $BaTiO_3$. After the absorption of the incoming photon, the system is left in an excited state (intermediate state) and two possible channels of deexcitation are possible (final state).

The RIXS processes at the origin of the elastic peak and of the CT feature are illustrated, in a single-particle picture, in Fig. 2. In both cases the core electron is excited to the conduction band. In the elastic process the same electron fills again the core hole, and the transition is described as $d^0 \rightarrow \underline{c}d^1 \rightarrow d^0$. In the CT process the core hole is filled by a valence electron, effectively producing an electron-hole excitation across the gap. Dipole selection rules would forbid a transition from the O $2p$ band to the $2p$ core hole, but, owing to the Ti $3d$-O $2p$ hybridization, the valence band has mixed orbital character, and the transition is therefore allowed. In a configuration-interaction picture, the ground state can be schematically described as $|GS\rangle = a|d^0\rangle + b|d^1\underline{L}\rangle$, where $\underline{L}$ stands for a hole in the ligand (O $2p$) band, and the coefficient b measures the strength of the hybridization. Conduction band states are antibonding states, generically represented as $|\epsilon\rangle = b|d^0\rangle - a|d^1\underline{L}\rangle$. The CT process corresponds to dipole-allowed transitions from the intermediate core state $\underline{c}d^1$ to the d^0 part of the $|\epsilon\rangle$ antibonding states, with intensity $I_{CT} \propto |b|^2$. The intensity of the CT signal in the RIXS spectrum is therefore a proxy for the Ti-O hybridization in the ground state, which we can exploit to follow changes in the hybridization at the paraelectric to ferroelectric phase transition, and in the low-temperature phases.

Figure 3 shows RIXS spectra measured in correspondence of the e_g XAS feature B at several temperatures between 445 K, in the paraelectric cubic phase, and 15 K, in the rhombohedral phase. They have been normalized to the same total integrated intensity I_0. The overall shape of the

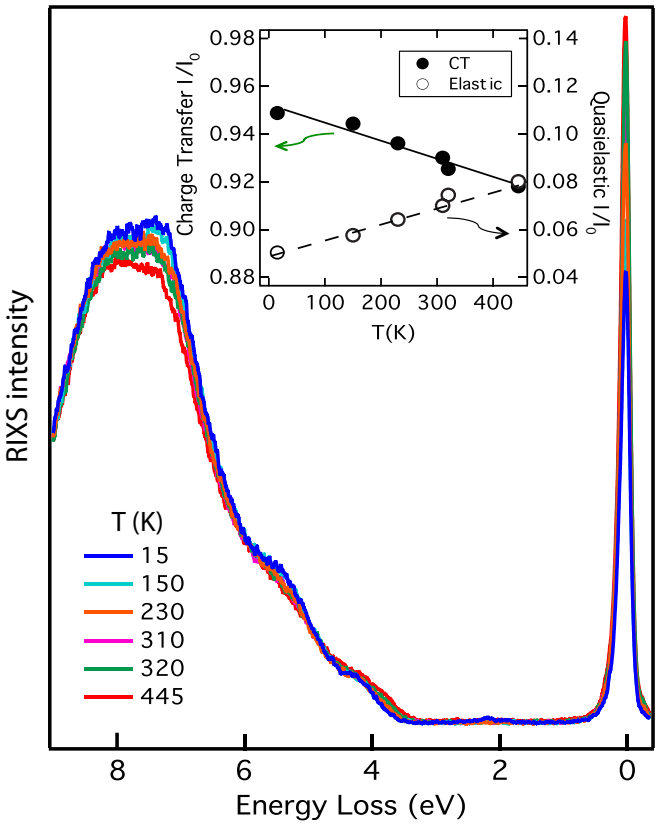

FIG. 3. RIXS data measured at selected temperatures between 445 K and 15 K, normalized to the same total integrated intensity I_0. The relative integrated intensities shown in the inset reveal a temperature-dependent spectral weight transfer between the quasielastic peak and the CT feature.

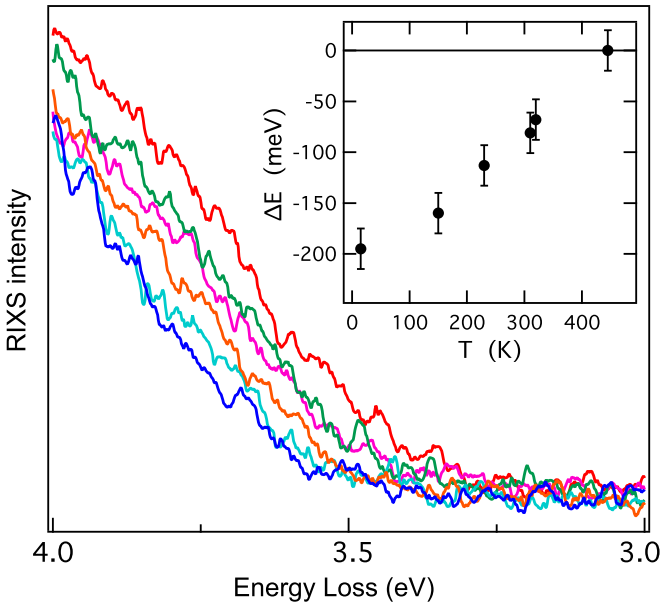

FIG. 4. Close up on the onset of the charge-transfer band, from Fig. 3. The inset shows the temperature-dependent shifts, determined by a linear extrapolation of the leading edge to the baseline. Error bars reflect uncertainties in the linear fit.

spectra is almost invariant but, as the temperature is lowered, the integrated intensity of the quasielastic peak is strongly reduced, by as much as 40% at 15 K. The loss of intensity cannot be ascribed to the freezing of unresolved low-energy excitations, such acoustic phonons. This would produce noticeable temperature-dependent changes of the line shape, which are not observed (see below). The missing intensity is indeed entirely transferred to the CT band, as illustrated by the inset, which shows the integrated quasielastic intensity and the intensity of the whole CT band, integrated in the 3 eV–12 eV range. The CT intensity increases by 3.5% with a statistical error of $\pm 0.2\%$ from high temperature to 15 K. The spectral weight transfer is linear over the whole temperature range, and there is no sign of discontinuity at T_C. Therefore, the data indicate that the Ti $3d$–O $2p$ hybridization exhibits a slight, continuous increase with reduced temperature. As a result of the larger hybridization we can also expect the CT gap, i.e., the separation between the (mainly) d^0 and $d^1\underline{L}$ manifolds, to increase. This is indeed confirmed by a closer look at the onset of the CT band, in Fig. 4. The temperature-dependent shifts of the spectral leading edge (inset) demonstrate a 0.2 eV gap widening between 445 K and 15 K. Our observations support first-principles calculations of the band structure suggesting the pivotal role of the Ti $3d$-O $2p$ hybridization in the ferroelectric instability [8]. On the other hand, the absence of any noticeable changes across T_C is consistent with the presence of local distortions already in the paraelectric cubic phase, and therefore supports the order-disorder scenario for the transition.

What is the origin of the increasing hybridization at low temperature? When the temperature varies from 445–15 K the lattice contracts by $\sim$0.6% [22]. This contraction produces a larger overlap of the wave functions, and therefore a larger hybridization. Assuming the validity of Harrison's $d^{-7/2}$ scaling relation for p-d hopping integrals [23], a uniform 0.6% contraction would yield a $\sim$2% increase in the hybridization. This in turn translates to an increase $\Delta I \sim 4\%$ of the CT signal in RIXS, which is quite close to the measured value. In $BaTiO_3$ the Ti-O distances are affected by the local distortion, which yields three short and three long Ti-O bonds in the rhombohedral phase. The overall increase in the hybridization is larger than for a uniform contraction. The relevant parameter $\langle d^{-7/2} \rangle$ averaged over all Ti-O distances increases by 1.9% between 300 K in the tetragonal phase, and 40 K [3], for an estimated 3.9% increase of the intensity of the CT signal. This is larger than the expected change for a uniform contraction (1.7%) in the same temperature range [22]. It is also larger than the $\Delta I \sim 2.1\%$ increase extracted from Fig. 3, but still in reasonable agreement, given the uncertainties of the crude model.

We now turn to the analysis of the low-energy excitations. Figure 1 shows that when the incident photon energy is varied along the XAS spectrum the quasielastic response changes not only in intensity, but also in width. For excitation energies up to the A_3 XAS feature (to the t_{2g} states) the peak is well described by a resolution-limited symmetric line shape. On the other hand, excitation into e_g orbitals yields a broader peak, with a distinctive tail. We have previously observed a similar photon energy dependence in Ti L-edge RIXS spectra of TiO_2

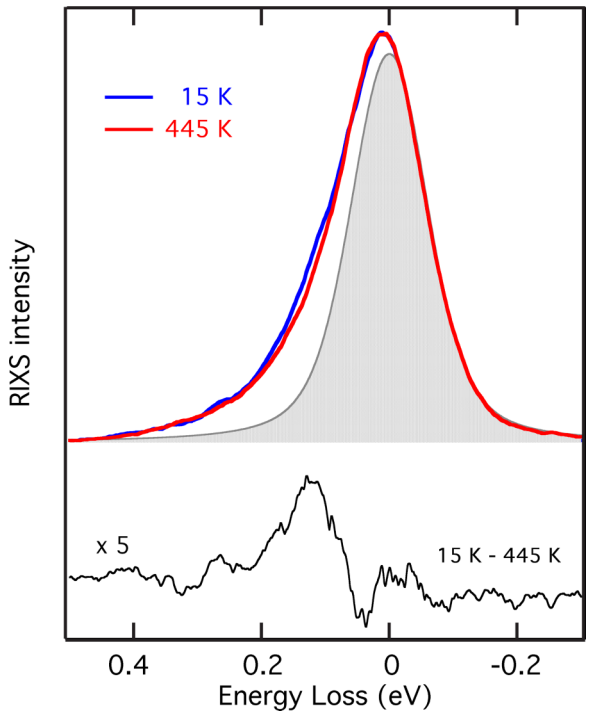

FIG. 5. (Top) Quasielastic response at 15 K and 445 K. The spectra have been normalized to the maximum intensity to compare their line shape. The symmetric peak centered at $E = 0$ is the resolution-limited elastic peak. (Bottom) 15 K–445 K difference spectrum, scaled by a factor 5.

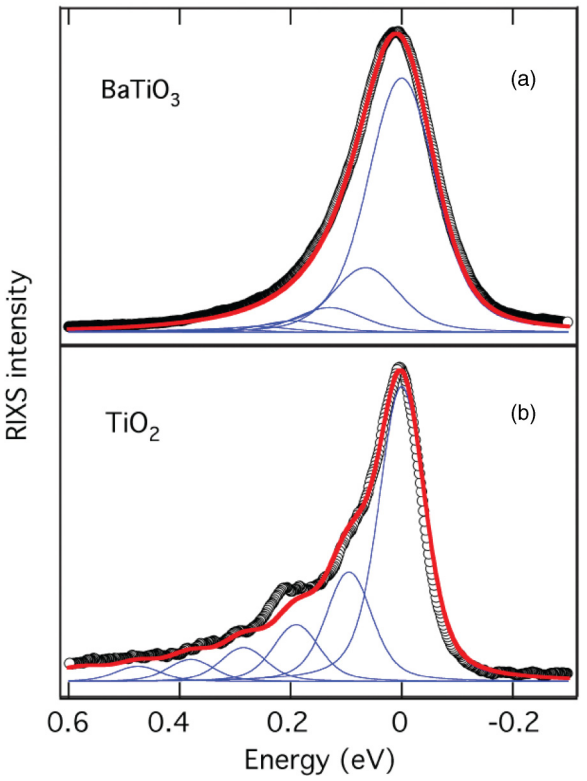

FIG. 6. (a) The thick red line is a fit of the RIXS quasielastic response (black symbols) of $BaTiO_3$ with the model of Ref. [16], for a TO phonon with $\hbar\omega_0 = 65$ meV and a coupling parameter $M = 250$ meV. Thin blue lines are the zero-loss peak and the phonon satellites. Lorentzian (FWHM = 375 meV) and Gaussian (FWHM = 135 meV) broadenings account for the core-hole lifetime and the experimental resolution. (b) Same for anatase TiO_2, with $\hbar\omega_0 = 95$ meV, $M = 480$ meV, and 110 meV Gaussian broadening.

anatase [17] and interpreted it as a consequence of the different nature of the intermediate states. Namely, the XAS feature A_3 has a strongly excitonic character, and the core hole potential is effectively screened by the localized $3d$ electron. As a result, after the filling of the core hole, the lattice is left in its ground state. By contrast, for excitation to the B XAS feature (to the e_g states) screening by the rather delocalized $3d$ electron is less effective, and the lattice is more strongly deformed. After the recombination, the lattice can be left in an excited vibrational state, and the phononic energy losses give rise to the tail of the quasielastic response observed in the RIXS spectra.

Figure 5 compares the quasielastic response measured for excitation at the XAS feature B at the highest (445 K) and lowest (15 K) temperatures. The spectra were normalized here to the same peak intensity in order to remove the large overall temperature effect discussed above and to enhance the visibility of changes in the line shape. The symmetric peak centered at $E = 0$ is the resolution-limited elastic peak. At both temperatures the spectra exhibit excess intensity to the left of the elastic peak, indicative of unresolved phononic losses. The line shape is quite similar, with a small enhancement at low temperature around 0.15 eV, which can be better appreciated in the difference spectrum.

Qualitatively the picture of phononic losses in RIXS is that of a displaced oscillator [24], which also describes the Franck-Condon effect in molecules. The zero-loss peak is followed by a progression of satellites separated by $\hbar\omega_0$, the energy of the relevant phonon mode. Similar spectral signatures have been observed in ARPES data of oxide materials [25–27].

Ament *et al.* [16] have calculated the RIXS spectral function in the presence of electron-phonon coupling for the Fröhlich Hamiltonian:

$$H = \sum_R M d_R^\dagger d_R (b_R^\dagger + b_R) + \sum_R \hbar\omega_0 b_R^\dagger b_R, \qquad (1)$$

where electrons are described by the fermionic operators $d_R^\dagger$ and phonons by the corresponding bosonic operators $b_R^\dagger$. M parametrizes the strength of the coupling to a mode of energy $\hbar\omega_0$. The Kramers-Heisenberg expression for the RIXS spectrum can be evaluated analytically for the case of a single Einstein phonon, and yields the intensities of the Franck-Condon satellites. Besides M and ω_0 the model contains as a parameter the inverse core hole lifetime Γ. For the Ti $2p_{3/2}$ core hole $\hbar\Gamma = 0.37$ eV [28].

We have applied the model of Ref. [16] to the quasielastic response of $BaTiO_3$. A difficulty of the analysis lies in the inability to resolve distinct losses in the phononic tail, which may indicate an unfavorable ratio of the phonon energy to the experimental energy resolution, or possibly the presence of several overlapping modes. RIXS selection rules are of no help here because, with the scattering geometry and light polarization of our experiment, all phonon mode symmetries present in the system can be observed in each phase. Since

the line shape is substantially temperature-independent we can assume that the same mode(s) is (are) excited at all temperatures. A prominent 65 meV TO Raman-active phonon is observed at all temperatures [5]. Therefore we set out to perform a minimal fit of the experimental spectrum with a single 65 meV mode. Such minimal fit does not exclude that other unresolved modes may contribute to the phononic loss tail. However, we do not expect the addition of further modes to significantly change our estimate of the electron-lattice coupling strength, encoded in the ratio of the inelastic to elastic intensities, which is the main goal of our analysis. The result of the fit, shown in Fig. 6(a) for a coupling constant $M = 250$ meV, is satisfactory. The blue lines in the figure represent the zero-loss peak at $E = 0$, and the phonon satellites separated by $\hbar\omega_0 = 65$ meV. The peaks have been broadened to account for the core-hole lifetime (FWHM = 375 meV, Lorentzian) and the experimental resolution (FWHM = 135 meV, Gaussian). The resulting spectrum (red line) provides a very good fit to the experimental data. Interestingly, the value of M extracted from the fit is quite close to the result of a completely independent analysis based on thermodynamic data that yields an electron-phonon interaction energy of 260 meV [29].

The main source of uncertainty attached to this value is the unknown intensity of the nonresonant contribution to the elastic peak, which is not considered by the model. Nevertheless, the photon energy dependence of Fig. 1 suggests that this contribution is small. To take this into account, we have then repeated the analysis after subtracting from the data an elastic contribution equal to 10% of the zero loss peak of Fig. 6(a), which most probably overestimates the nonresonant contribution. We could achieve an equally good fit (not shown) for $M = 300$ meV, which we consider an extreme upper limit to the coupling constant. The strength of the electron-phonon coupling can be expressed in terms of the dimensionless ratio $M/\hbar\omega_0$ between the coupling constant and the energy of the phonon. Our fit yields $M/\hbar\omega_0 = 3.8$–4.6, which places $BaTiO_3$ at the boundary between the intermediate and strong coupling regimes [30].

It is interesting to compare our results for $BaTiO_3$ with data on anatase, another Ti oxide where e-ph coupling is responsible for the formation of large polarons, which influence transport and spectroscopic properties [17,27]. Figure 6(b) shows the RIXS spectrum of anatase, also measured at the XAS transition to the e_g states. In this case it is possible to identify at least two satellites, owing to a larger energy separation and to a better experimental resolution (110 meV). A cursory analysis of the data shows that the phononic tail decays more slowly than in $BaTiO_3$. In particular, the intensity ratio of the second to the first satellite, which, according to theory is proportional to M^2, appears to be larger in anatase. This is confirmed by a full calculation, which yields the spectrum (red line) and the Franck-Condon satellites (blue lines) shown in the figure for a coupling parameter $M = 480$ meV, yielding $M/\hbar\omega_0 \sim 5$. The comparison indicates that e-ph coupling is indeed stronger in TiO_2 anatase, which can be considered as a benchmark material for moderately strong coupling [31].

In summary, we exploited soft x-ray RIXS to investigate the electronic structure over a broad temperature range and the coupling to the lattice in the ferroelectric material $BaTiO_3$. We found that the Ti-O hybridization increases continuously with decreasing temperature, owing to the combined result of thermal contraction and local distortion leading to the formation of three short Ti-O bonds in the distorted TiO_6 octahedra. We find no evidence of a discontinuity at the paraelectric to ferroelectric transition. Our observations support the existence of randomly oriented electric dipoles already in the paraelectric phase, and the order-disorder model of the transition. We also found spectral signatures of phonon losses in the quasielastic response. A minimal fit of the line shape with a single 65 meV TO phonon, yields a satisfactory description of the experimental data. From that analysis we extract a dimensionless coupling parameter $M/\hbar\omega_0 \sim 4$, corresponding to an intermediate coupling strength. More generally, the present results confirm that soft x-ray RIXS is a sensitive probe of the electronic states and of collective excitations in transition metal oxides.

ACKNOWLEDGMENTS

This work has been supported by the Swiss NSF. Work at SPring-8 is jointly supported by the Synchrotron Radiation Research Organization and the Institute for Solid State Physics, the University of Tokyo (Proposal No. 2015B7499). S.M. acknowledges support of the Swiss NSF under Grant No. P2ELP2-155357.

[1] M. E. Lines and A. M. Glass, *Principles and Applications of Ferroelectrics and Related Materials* (Clarendon Press, Oxford, 1977).
[2] R. Comès, M. Lambert, and A. Guinier, Acta Crystallogr. Sect. A **26**, 244 (1970).
[3] B. Ravel, E. A. Stern, R. I. Vedrinskii, and V. Kraizman, Ferroelectrics **206**, 407 (1998).
[4] I. Levin, V. Krayzman, and J. C. Woicik, Phys. Rev. B **89**, 024106 (2014).
[5] J. Parsons and L. Rimai, Solid State Commun. **5**, 423 (1967).
[6] M. S. Senn, D. A. Keen, T. C. A. Lucas, J. A. Hriljac, and A. L. Goodwin, Phys. Rev. Lett. **116**, 207602 (2016).
[7] D. I. Khomskii, *Transition Metal Compounds* (Cambridge University Press, Cambridge, 2014).
[8] R. E. Cohen, Nature (London) **358**, 136 (1992).
[9] J. J. Wang, F. Y. Meng, X. Q. Ma, M. X. Xu, and L. Q. Chen, J. Appl. Phys. **108**, 034107 (2010).
[10] A. Chassé, S. Borek, K.-M. Schindler, M. Trautmann, M. Huth, F. Steudel, L. Makhova, J. Gräfe, and R. Denecke, Phys. Rev. B **84**, 195135 (2011).
[11] K. Yoshii *et al.*, J. Phys. Chem. Solids **75**, 339 (2014).
[12] L. J. P. Ament, M. van Veenendaal, T. P. Devereaux, J. P. Hill, and J. van den Brink, Rev. Mod. Phys. **83**, 705 (2011).
[13] S. Fatale, S. Moser, and M. Grioni, J. Electron Spectrosc. Relat. Phenom. **200**, 274 (2015).
[14] F. Hennies, A. Pietzsch, M. Berglund, A. Föhlisch, T. Schmitt, V. Strocov, H. O. Karlsson, J. Andersson, and J.-E. Rubensson, Phys. Rev. Lett. **104**, 193002 (2010).

[15] W. S. Lee, S. Johnston, B. Moritz, J. Lee, M. Yi, K. J. Zhou, T. Schmitt, L. Patthey, V. Strocov, K. Kudo, Y. Koike, J. van den Brink, T. P. Devereaux, and Z. X. Shen, Phys. Rev. Lett. **110**, 265502 (2013).
[16] L. J. P. Ament, M. van Veenendaal, and J. van den Brink, Europhys. Lett. **95**, 27008 (2011).
[17] S. Moser, S. Fatale, P. Krüger, H. Berger, P. Bugnon, A. Magrez, H. Niwa, J. Miyawaki, Y. Harada, and M. Grioni, Phys. Rev. Lett. **115**, 096404 (2015).
[18] K. Yoshii *et al.*, J. Phys. Chem. Solids **73**, 1106 (2012).
[19] Y. Harada, M. Kobayashi, H. Niwa, Y. Senba, H. Ohashi, T. Tokushima, Y. Horikawa, S. Shin, and M. Oshima, Rev. Sci. Instrum. **83**, 013116 (2012).
[20] F. M. F. de Groot, J. C. Fuggle, B. T. Thole, and G. A. Sawatzky, Phys. Rev. B **41**, 928 (1990).
[21] P. Krüger, Phys. Rev. B **81**, 125121 (2010).
[22] M. Han *et al.*, Crys. Eng. Commun. **17**, 1944 (2015).
[23] W. A. Harrison, *Electronic Structure and the Properties of Solids* (Dover, New York, 1989).
[24] G. D. Mahan, *Many-Particle Physics*, 2nd ed. (Plenum, New York, 1993).
[25] D. S. Dessau, T. Saitoh, C.-H. Park, Z.-X. Shen, P. Villella, N. Hamada, Y. Moritomo, and Y. Tokura, Phys. Rev. Lett. **81**, 192 (1998).
[26] K. M. Shen, F. Ronning, D. H. Lu, W. S. Lee, N. J. C. Ingle, W. Meevasana, F. Baumberger, A. Damascelli, N. P. Armitage, L. L. Miller, Y. Kohsaka, M. Azuma, M. Takano, H. Takagi, and Z. X. Shen, Phys. Rev. Lett. **93**, 267002 (2004).
[27] S. Moser, L. Moreschini, J. Jaćimović, O. S. Barišić, H. Berger, A. Magrez, Y. J. Chang, K. S. Kim, A. Bostwick, E. Rotenberg, L. Forró, and M. Grioni, Phys. Rev. Lett. **110**, 196403 (2013).
[28] J. C. Fuggle and S. F. Alvarado, Phys. Rev. A **22**, 1615 (1980).
[29] E. Iguchi, A. Tamenori, and N. Kubota, Phys. Rev. B **45**, 697 (1992).
[30] S. N. Klimin and J. T. Devreese, Phys. Rev. B **89**, 035201 (2014).
[31] In Ref. [17] an incorrect implementation of the model led us to a quantitatively inaccurate estimate $M = 130$ meV.